Vertical structure of the atmosphere

Thermodynamics, Radiative transfer, Radiative-convective equilibrium

Vertical structures of planetary atmospheres

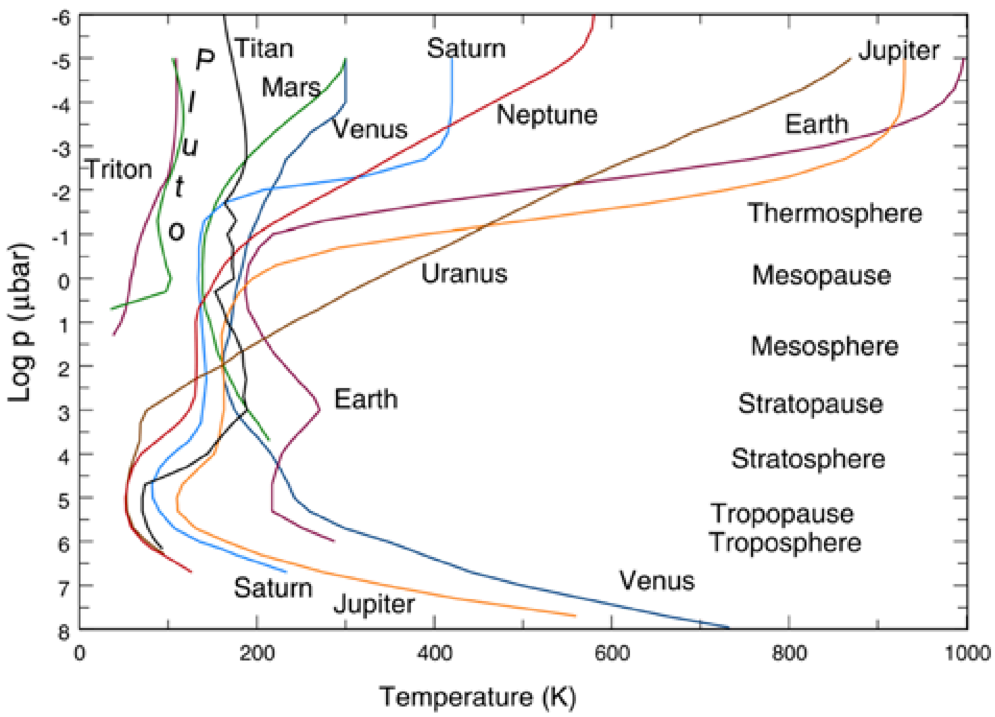

(Mueller-Wodarg et al.)

Hydrostatic equilibrium

The gravitational acceleration is assumed to be a constant value g.

The balance between the pressure gradient force and the gravitational acceleration in the vertical direction is

$$-S\Delta p = g\rho S\Delta z$$

$$\therefore \frac{dp}{dz} = -g\rho \qquad (1.1)$$

p: pressure z : altitude ρ: mass density (kg/m^3)

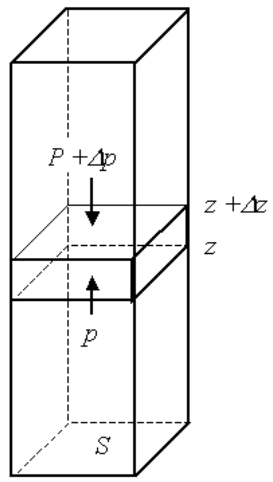

This is equivalent to the vertical momentum equation

$$\frac{dw}{dt} = -\frac{1}{\rho}\frac{\partial p}{\partial z} - g$$

except that the vertical wind w is assumed to be zero.

Integrating (1.1) we have

$$p(z) = \int_z^\infty g\rho(z')dz'$$

The equation of state:

$$p = \rho RT \qquad (1.2)$$

R : gas constant (= 287 J/K/kg for Earth)
$R = k/m$, where k is Boltzmann's constant and m is the mean mass of molecules

Combining (1.1) (1.2), we have

$$\frac{dp}{dz} = -\frac{gp}{RT}$$

$$\therefore p(z) = p_S \exp\left(-\int_0^z \frac{dz'}{H(z')}\right)$$

p_s : surface pressure
$H = RT/g$: scale height (6-8km on Earth)
(~16 km on Venus, ~11 km on Mars)

When the temperature is constant with altitude,

$$p(z) = p_S \exp\left(-\frac{z}{H}\right)$$

Horizontally-thin layers tend to prevail in planetary atmospheres.

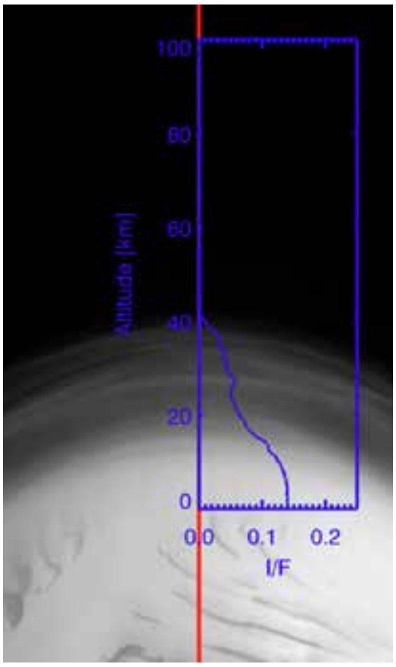

Haze layer of Mars
(Stenzel et al. 2011)

Haze layer of Titan

→ Air parcels tend to stay at constant levels in a stably-stratified atmosphere.

Thermodynamics

First law of thermodynamics:

$$dH = c_v dT + p d\alpha \qquad (2.1)$$

dH : heat given to gas of unit mass
c_v : specific heat for constant volume
$\alpha = 1/\rho$: specific volume

Combined with the state equation $p\alpha = RT$, we obtain

$$p d\alpha + \alpha dp = R dT \qquad (2.2)$$

Combining (2.1)(2.2) yields

$$dH = c_p dT - \alpha dp \qquad (2.3)$$

$c_p = c_v + R$: specific heat for constant pressure

Considering a diabatic process (dH = 0), we have

$$c_p dT = \frac{RT}{p} dp$$

$$c_p d(\ln T) = R d(\ln p)$$

$$\therefore T = const. \times p^{R/C_p}$$

Therefore, the potential temperature θ which is defined as

$$\theta \equiv T\left(\frac{p_S}{p}\right)^{R/C_p} \qquad (2.4)$$

is conserved in adiabatic processes.

In adiabatic ascent or decent, θ is constant with altitude. In this case, under hydrostatic equilibrium, we obtain

$$\frac{dT}{dz} = -\frac{g}{c_p} = -\Gamma_d \qquad (2.5)$$

Γ_d : dry adiabatic lapse rate (9.8 K/km on Earth)

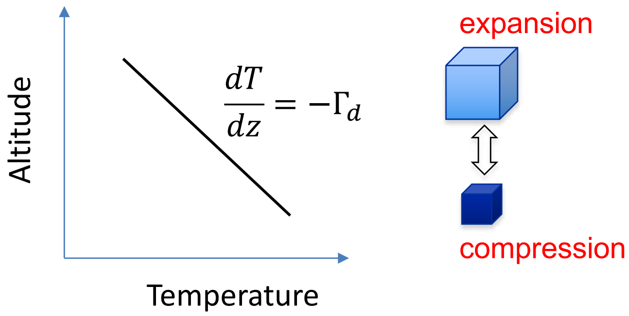

Static stability

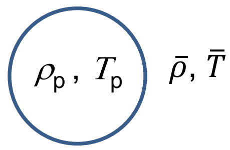

The buoyancy acting on an air parcel is given by

$$\frac{d^2 z}{dt^2} = g\frac{\bar{\rho} - \rho_p}{\rho_p}$$

z : altitude of the air parcel
$\bar{\rho}$: mass density of ambient air
ρ_p : mass density of the air parcel

Assuming that the pressures of the air parcel and the ambient atmosphere are equal, we have

$$\frac{d^2 z}{dt^2} = g\frac{\bar{T}^{-1} - T_p^{-1}}{T_p^{-1}} = g\frac{T_p - \bar{T}}{\bar{T}} \qquad (2.6)$$

$\bar{T}$: ambient temperature
T_p : temperature of air parcel

Temperatures are expressed by using the temperature T_0 at the original position (z=0):

$$\bar{T} = T_0 - \Gamma z$$
$$T_p = T_0 - \Gamma_d z \qquad (2.7)$$

$\Gamma = -d\bar{T}/dz$: ambient lapse rate

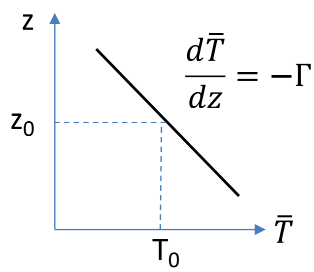

From (2.6)(2.7)

$$\frac{d^2 z}{dt^2} \sim -g \frac{\Gamma_d - \Gamma}{T_0} z$$

When Γ_d - Γ is positive, an oscillating solution exists.
The buoyancy frequency *N* is given by

$$N^2 = g \frac{\Gamma_d - \Gamma}{T_0} = g \frac{\partial \ln \overline{\theta}}{\partial z}$$

Three types of static stability:

$\Gamma_d - \Gamma > 0 \leftrightarrow S > 0 \leftrightarrow \partial\bar{\theta}/\partial z > 0$: stable
$\Gamma_d - \Gamma = 0 \leftrightarrow S = 0 \leftrightarrow \partial\bar{\theta}/\partial z = 0$: neutral
$\Gamma_d - \Gamma < 0 \leftrightarrow S < 0 \leftrightarrow \partial\bar{\theta}/\partial z < 0$: unstable

$S = dT/dz + \Gamma_d$: Static stability

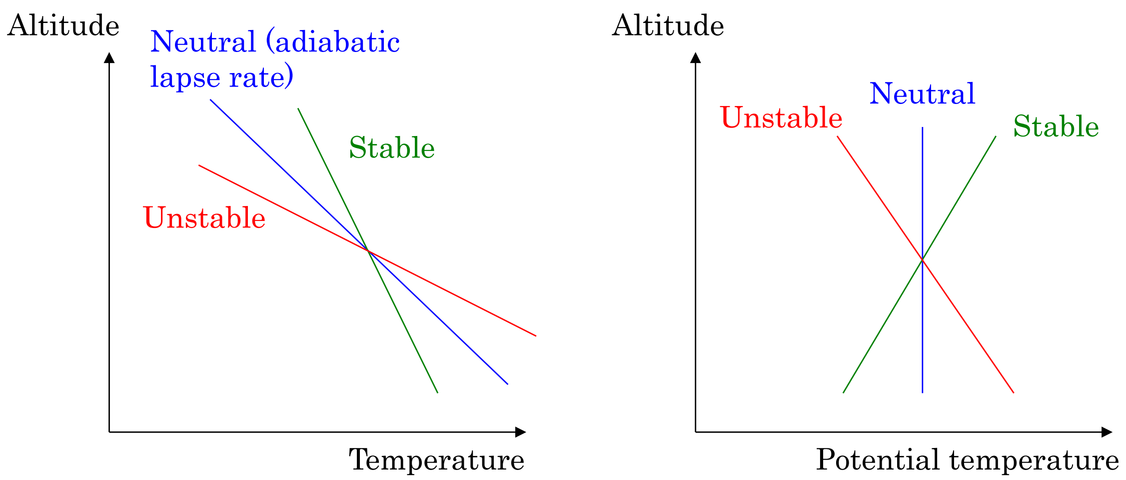

Stability of Earth’s atmosphere

Gettelman et al. (2011)

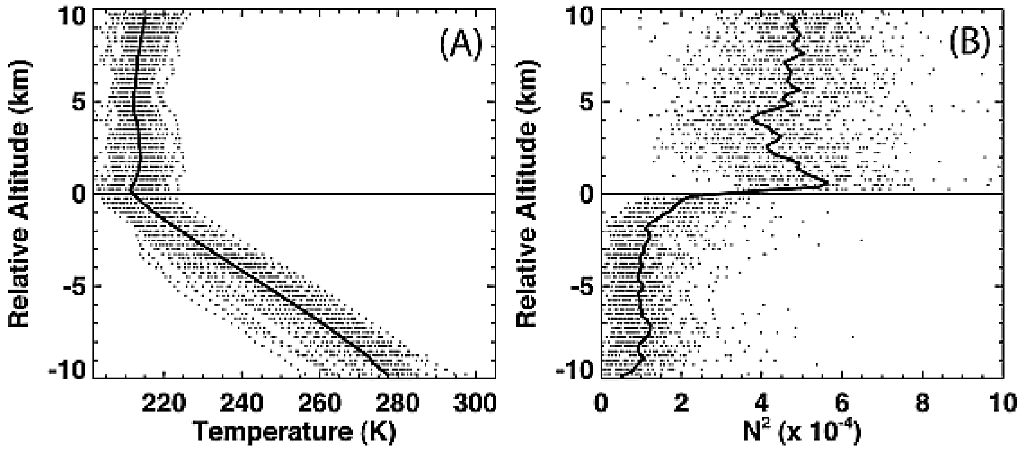

Stability of Venusian atmosphere

Neutral layer exists around 50-60 km in the cloud

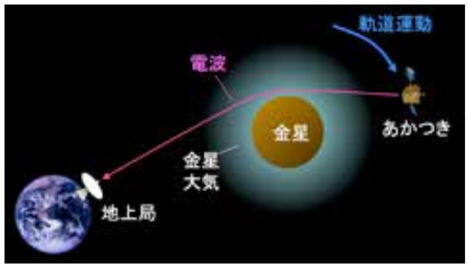

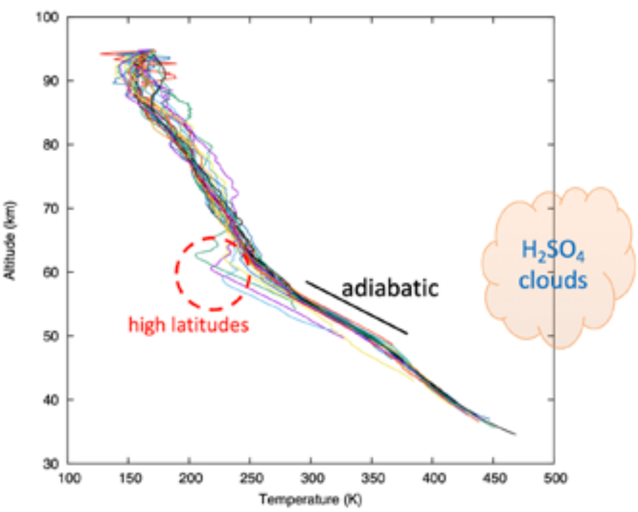

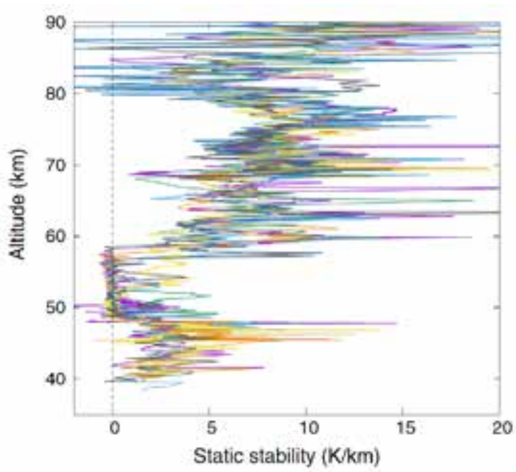

Akatsuki radio occultation (Imamura et al. 2017)

Stability of Martian atmosphere

Mixed boundary layer (Hinson et al. 2008)

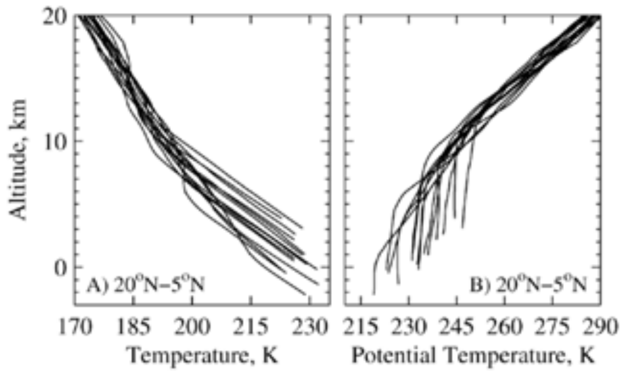

Detached mixed layer
(Hinson et al. 2014)

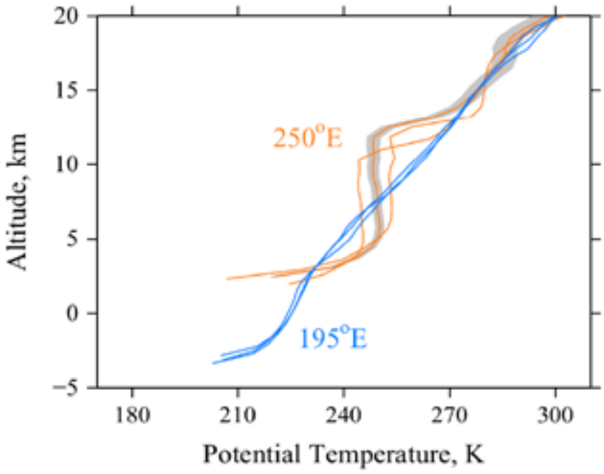

Radiation

Energy balance of a planet

Inflow : Visible wavelength radiation from Sun

Outflow : Infrared radiation from the surface and the atmosphere

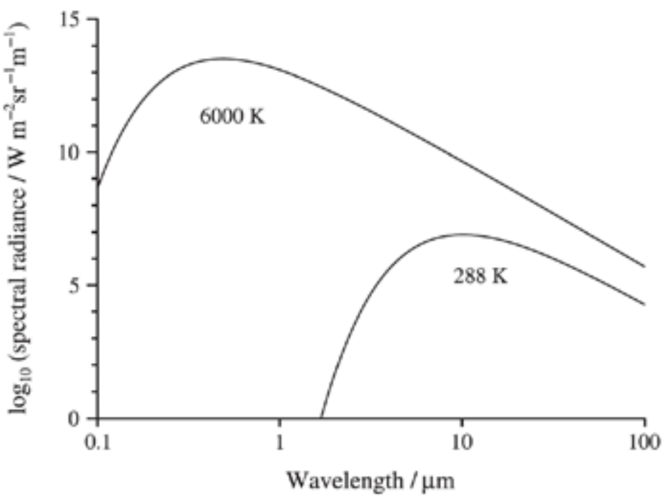

Andrews (2000)

Logarithm of the black-body spectral radiance $B_\lambda(T)$, plotted against the logarithm of wavelength λ, for $T = 6000$ K, a typical temperature of the solar photosphere, and 288 K, the Earth's mean surface temperature.

Radiance/Intensity

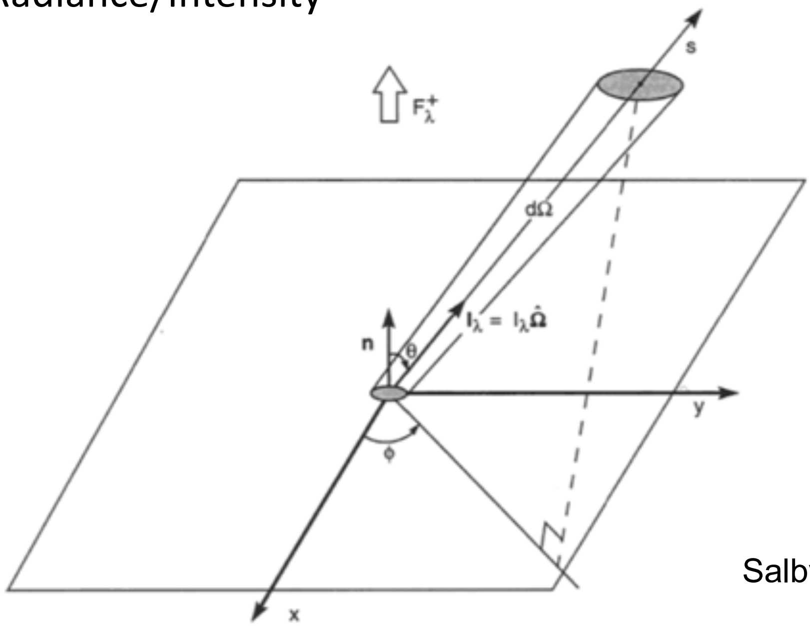

Salby (1996)

Figure 8.6 A pencil of radiation that occupies the increment of solid angle $d\Omega$ in the direction $\hat{\Omega}$ and traverses a surface with unit normal $\boldsymbol{n}$. The monochromatic *intensity* or *radiance* passing through the pencil: $\boldsymbol{I}_\lambda = I_\lambda \hat{\boldsymbol{\Omega}}$, describes the rate at which energy inside the pencil crosses the surface per unit area, steradian, and wavelength. Integrating the component normal to the surface: $I_\lambda(\hat{\boldsymbol{\Omega}} \cdot \boldsymbol{n}) = I_\lambda \cos\theta$, over the half-space of 2π steradians in the positive $\boldsymbol{n}$ direction yields the monochromatic forward *flux* or *irradiance* F_λ^+.

Planck function（J/m2/s/str/Hz）

$$B_\nu(T) = \frac{2h\nu^3}{c^2(e^{h\nu/kT} - 1)}$$

h: Planck's constant
ν: frequency
c : speed of light
k : Boltzmann's constant

Integration for wavelength and for solid angle over a hemisphere

$$\underbrace{\int_0^{2\pi} d\phi \int_0^{\pi/2} d\theta \sin\theta\cos\theta}_{\text{Integration for solid angle}} \ \underbrace{\int_0^\infty d\nu}_{\text{Integration for frequency}} B_\nu(T) = \pi \int_0^\infty d\nu B_\nu(T) = \sigma T^4$$

Integration for solid angle

Integration for frequency

σ : Stefan-Boltzmann's constant

Equilibrium between solar radiation and planetary infrared radiation

$$(1-A)\,\pi\, a^2\, S = 4\pi\, a^2\, \sigma\, T^4$$

A: albedo (0.3 for Earth)
a : planetary radius
S: solar constant（1370 W m^{-2} for Earth）

For Earth, T＝255 K : "effective temperature"

Interaction between electromagnetic waves and molecules

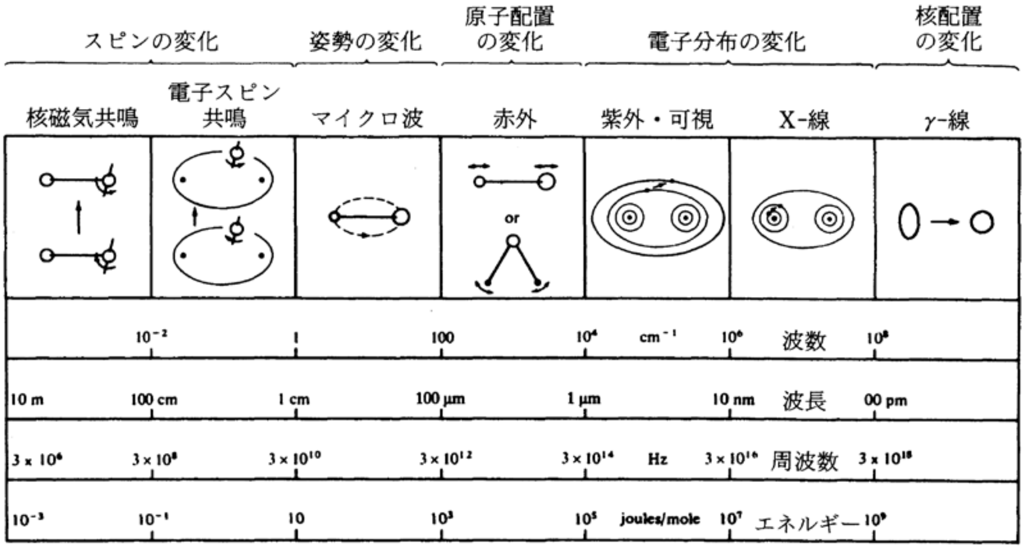

図 5.1 電磁波のスペクトルと電磁波–分子 (原子) の相互作用のメカニズム (Banwell and McCash, 1994)[26]

柴田（1999）

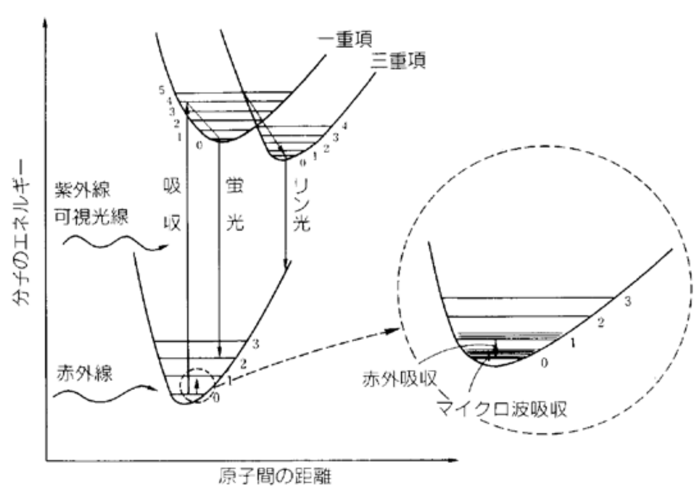

図 1-3 分子のエネルギーレベルと光の吸収

柴田（1999）

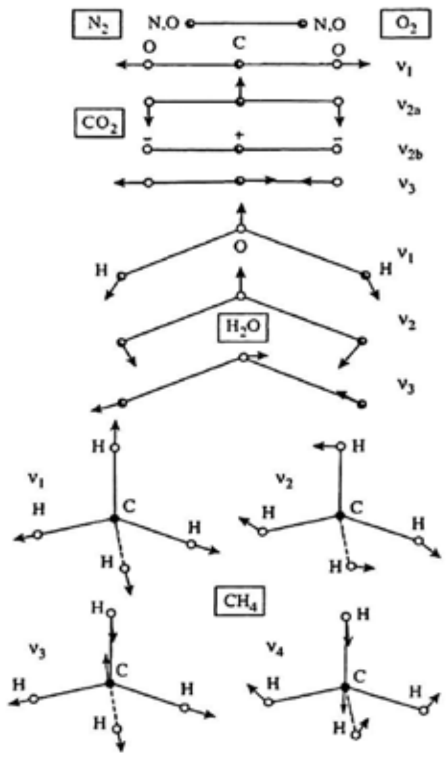

Catling & Kasting (2017)

Vibrational energy levels

$$E_v = h\nu_0\left(v + \frac{1}{2}\right)$$

v : vibrational quantum number

Rotational energy levels

$$E_J = hB(\,J(J+1))$$

J : rotational quantum number

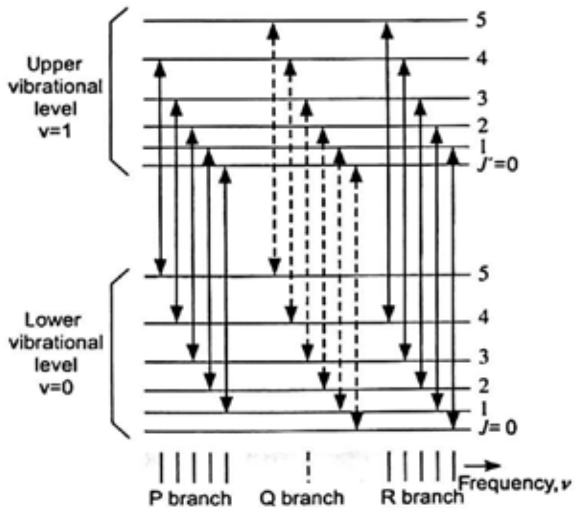

Figure 2.23 The meaning of the P, Q, and R branches in vibrational–rotational transitions, showing a vibrational transition Δv and superposed rotational transitions, ΔJ. The P branch corresponds to Δv =1 with rotational transitions ΔJ = −1. The Q branch corresponds to Δv =1 and ΔJ = 0 and the R branch corresponds to Δv =1 and ΔJ = +1. The lower shaded panel shows the appearance of the lines in the spectrum schematically, noting that the Q branch is offset from P and R branches for clarity in order to show the Q-branch ΔJ transitions.

Catling & Kasting (2017)

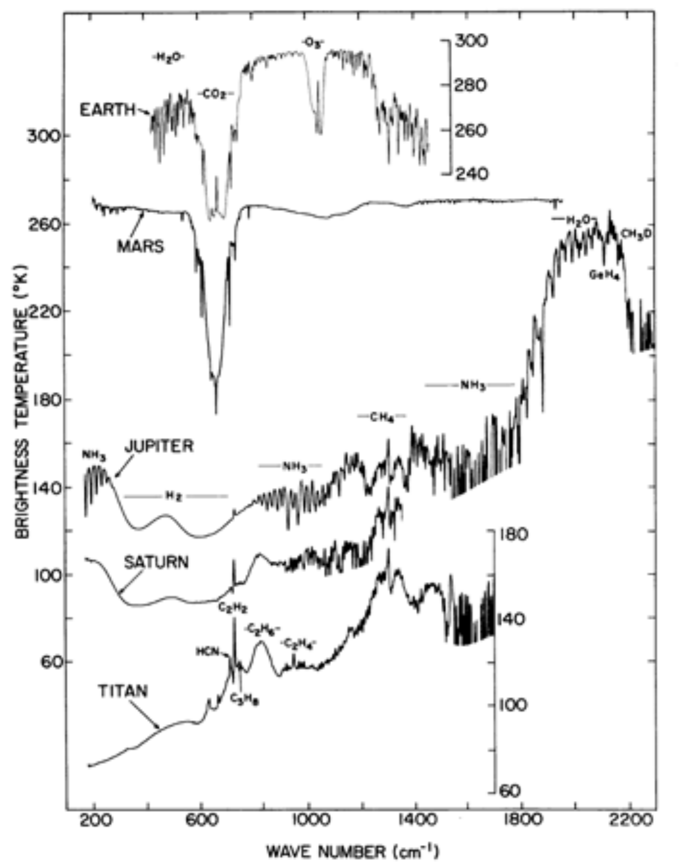

Chamberlain & Hunten (1987)

Fig. 4.21 Spectra in the thermal infrared, plotted as brightness temperatures, for four planets and Titan. Features that show as "absorptions" are formed in a region of negative temperature gradient (troposphere); those that show as "emissions" are from a warm stratosphere. [After Hanel (1983).]

Radiative transfer in plane-parallel atmosphere

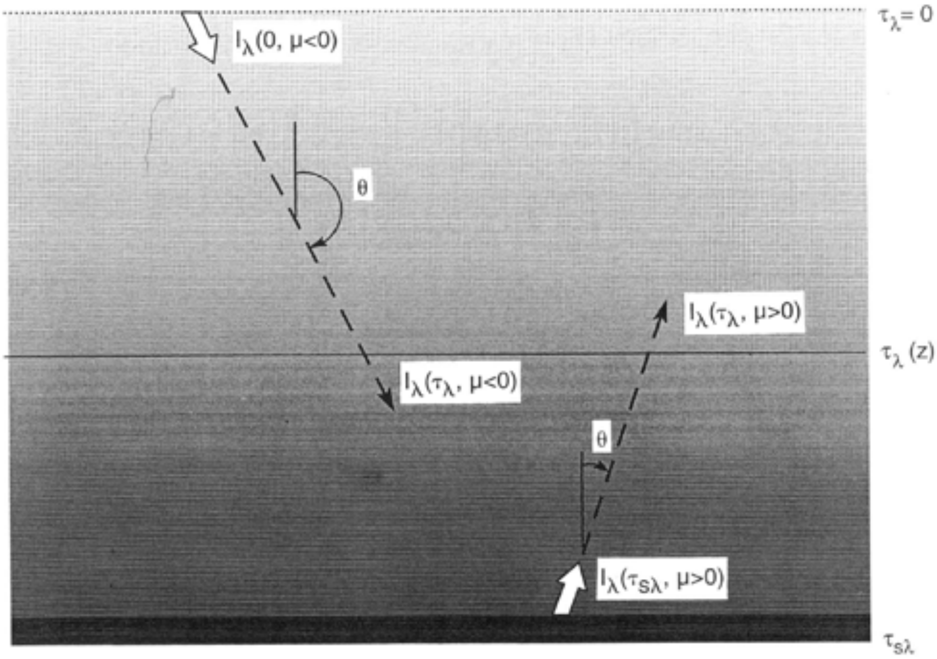

Figure 8.17 Plane parallel atmosphere, in which a pencil of radiation is inclined at the zenith angle $\theta = \cos^{-1}\mu$. Elevation is measured by the optical depth for a given wavelength τ_λ, which increases downward from zero at the top of the atmosphere to a surface value of $\tau_{s\lambda}$.

Salby (1996)

Radiative transfer equation

$$dI = (absorption) + (emission) = -k_a I ds + k_a B(T) ds$$

$$\therefore \frac{dI}{k_a ds} = -I + B(T)$$

I : radiance (J/m2/s/str/Hz)
k_a : absorption coefficient
s : coordinate along the ray

Optical depth

$$\tau = \int_z^\infty k_a dz'$$

Equation for radiance with the zenith angle of θ （μ＝cosθ）

$$\mu \frac{dI}{d\tau} = I - B$$

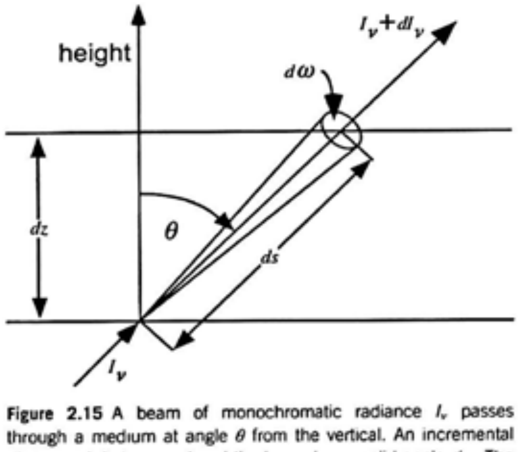

Figure 2.15 A beam of monochromatic radiance I_ν passes through a medium at angle θ from the vertical. An incremental distance ds is traversed and the beam has a solid angle $d\omega$. The vertical incremental distance is $dz = ds\cos\theta$.

Catling & Kasting (2017)

Upward radiance at the top of the atmosphere

$$I = B(T_S)\exp(-\tau_s) + \int_0^{\tau_s} B(T(\tau))\exp(-\tau)\,d\tau$$

$$= B(T_s)\exp(-\tau_s) + \int_0^{\infty} B(T(z))\,k_a(z)\exp(-\tau(z))\,dz$$

Contribution function

From surface

From atmosphere

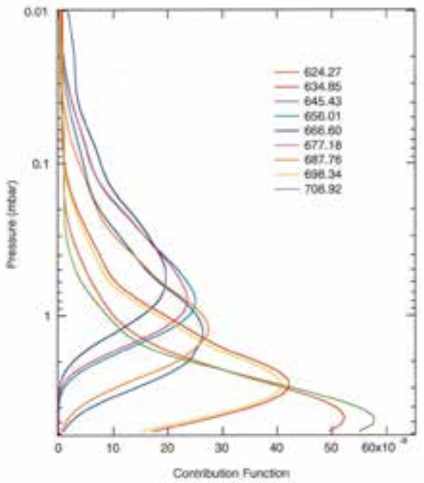

Plate 1. Contribution functions (functional derivatives of radiance with respect to temperature) for the wavenumbers used in the temperature retrievals. These functions were calculated using (10) and are for the nominal Thermal Emission Spectrometer (TES) 10 cm^{-1} resolution. Units for the contribution functions are W cm^{-2} sr^{-1} cm^{-1} K^{-1}.

Contribution functions for Mars atmosphere in infrared（Conrath et al. 2000）

Temperature distribution retrieved from Marg Global Surveyor TES spectra (Smith et al. 2001)

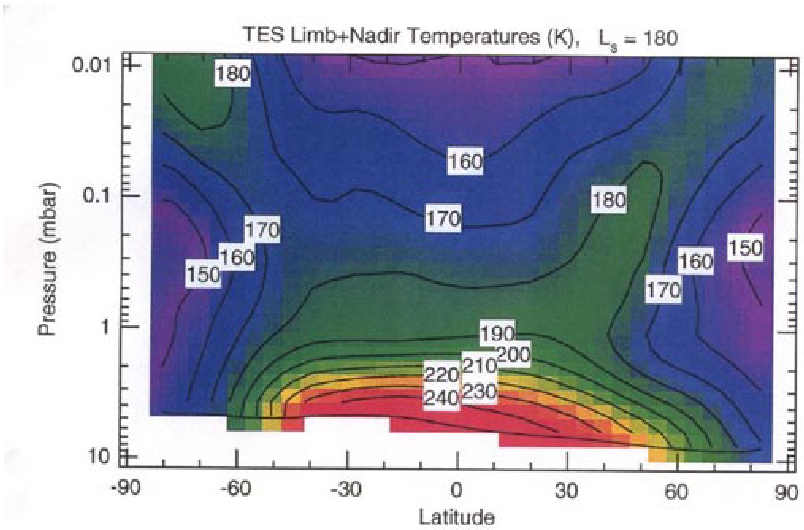

Contribution functions for Venus atmosphere（Schofield & Taylor 1983）

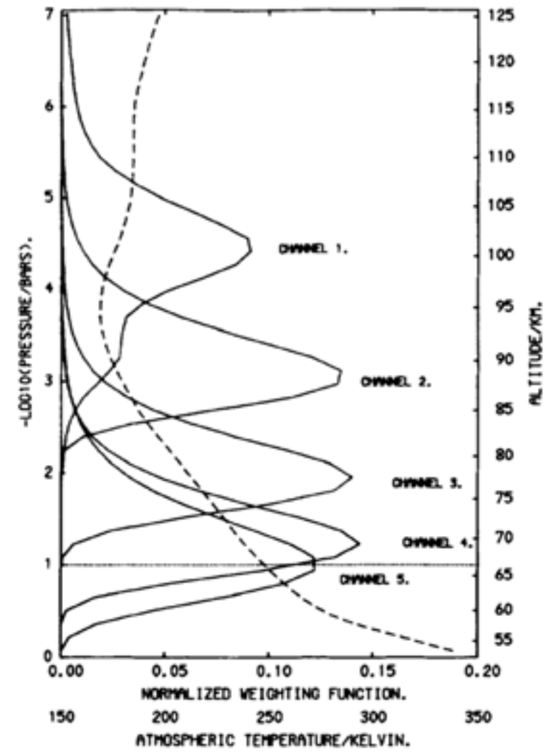

TABLE 1. OIR TEMPERATURE-SOUNDING CHANNELS – OPTICAL PROPERTIES

Channel*	Field of view** full angle (degrees)	Effective wavelength† (cm⁻¹)	Effective wavelength† (μm)	Spectral resolution†† (cm⁻¹)
1	5·0	667·0	15·0	0·005
2	1·25	679·4	14·7	10·7
3	1·25	727·2	13·8	12·0
4	1·25	764·4	13·1	14·3
5	1·25	872·0	11·5	22·3

Obtained temperature distribution of Venus atmosphere（Schofield & Taylor 1983）

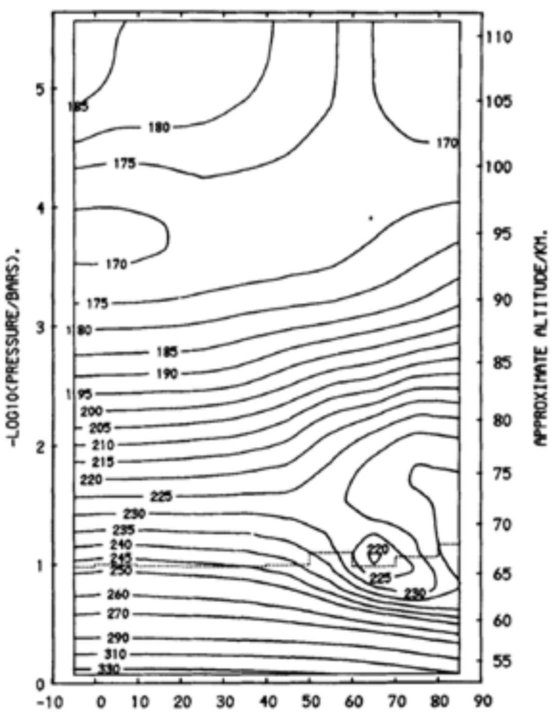

Figure 9. The retrieved zonal-mean temperature field and cloud structure. The temperature field is contoured as a function of pressure and latitude, and the altitude scale is averaged over latitude. Cloud unit optical depth at 11·5 μm is indicated by a dotted line.

Upward/downward flux（θ’ = π－θ)（μ = cosθ）

$$F^{\uparrow} = \int_0^{2\pi} d\phi \int_0^{\pi/2} I(\theta)\cos\theta\sin\theta\, d\theta = 2\pi\int_0^1 I(\mu)\mu\, d\mu = \pi\int_0^1 I(\mu)\mu\, d\mu \Big/ \int_0^1 \mu\, d\mu$$

$$F^{\downarrow} = \int_0^{2\pi} d\phi \int_0^{\pi/2} I(\theta')\cos\theta'\sin\theta' d\theta' = -2\pi\int_{-1}^0 I(\mu)\mu\, d\mu = \pi\int_{-1}^0 I(\mu)\mu\, d\mu \Big/ \int_{-1}^0 \mu\, d\mu$$

Two-stream approximation：

$$F^{\uparrow} = \pi I(\overline{\mu})$$

$$F^{\downarrow} = \pi I(-\overline{\mu})$$

$$\tau^* = \overline{\mu}^{-1}\tau$$

$$B^* = \pi B$$

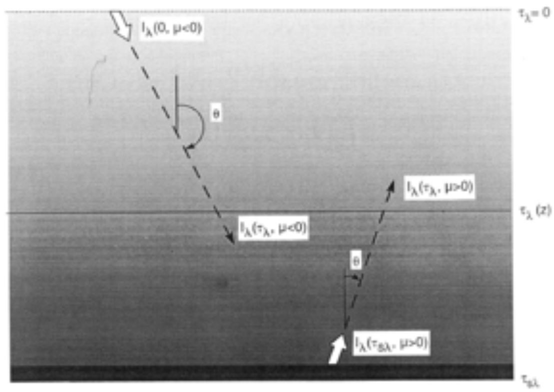

Figure 8.17 Plane parallel atmosphere, in which a pencil of radiation is inclined at the zenith angle $\theta = \cos^{-1}\mu$. Elevation is measured by the optical depth for a given wavelength τ_λ, which increases downward from zero at the top of the atmosphere to a surface value of $\tau_{s\lambda}$.

We have

$$\frac{dF^{\uparrow}}{d\tau^*} = F^{\uparrow} - B^*$$

$$-\frac{dF^{\downarrow}}{d\tau^*} = F^{\downarrow} - B^* \qquad (3.1)$$

$\overline{\mu} \approx 3/5$, corresponding to the zenith angle of 53°, is frequently adopted.

Radiative equilibrium in gray atmosphere

・Absorption coefficient in infrared does not depend on the wavelength.

・The atmosphere is transparent for solar radiation (visible wavelength)

・Solar energy reaching the surface is converted to thermal emission.

・Plane-parallel atmosphere with the incoming solar flux of F_0:

$$F_0 = (1 - A)\frac{S}{4}$$

S : solar constant
A : albedo

Substituting

$F^{net} = F^{\uparrow} - F^{\downarrow}$: net upward flux

$F^{sum} = F^{\uparrow} + F^{\downarrow}$: total flux

into (3.1), we obtain

$$\frac{dF^{net}}{d\tau^*} = F^{sum} - 2B^* \qquad (3.2)$$

$$\frac{dF^{sum}}{d\tau^*} = F^{net} \qquad (3.3)$$

F^{net} is equal to the incoming solar flux F^0 :

$$F^{net} = F^0 \quad (3.4)$$: Net flux is invariant

From (3.2)(3.4)

$$F^{sum} = 2B^* \quad (3.5)$$: Total flux is determined by the local temperature

From (3.3)(3.4)

$$F^{sum} = F^0\tau^* + F^{sum}(\tau^* = 0) \quad (3.6)$$

From (3.5)(3.6)

$$B^*(\tau^*) = \frac{F^0}{2}\tau^* + \frac{F^{sum}(\tau^* = 0)}{2} \quad (3.7)$$

Since $F^{\downarrow} = 0$ at the top of the atmosphere ($\tau^* = 0$)

$$F^{sum}(\tau^* = 0) = F^{net} = F^0 \quad (3.8)$$

From (3.7)(3.8)

$$B^*(\tau^*) = \frac{F^0}{2}(\tau^* + 1) \quad (3.9)$$

Considering $B^* = \sigma T^4$, the temperature increases with decreasing the altitude (greenhouse effect).

Large τ can lead to high temperatures→ Venus's atmosphere

The temperature at the top of the atmosphere ($\tau^*=0$) is

$$T = \left(F^0/2\sigma\right)^{1/4}$$: "skin temperature" = temperature of the stratosphere

This value is lower than the effective temperature.

From (3.4)(3.5) and the definition of F^{net} and F^{sum}, we obtain

$$F^{\downarrow} = \frac{F^{sum} - F^{net}}{2} = B^* - \frac{F^0}{2} \quad (3.10)$$

Emission from the surface is equal to the sum of the solar flux reaching the surface and the downward emission from the atmosphere:

$$B^*(T_S) = F^0 + F^{\downarrow}(\tau_s^*) \quad (3.11)$$ T_S: surface temperature
τ_S: optical depth at the surface

From (3.10)(3.11), we obtain

$$B^*(T_S) = B^*(\tau_s^*) + \frac{F^0}{2}$$

surface ($B^*(T_S)$); bottom of atmosphere ($B^*(\tau_s^*)$)

→ Temperature discontinuity exists at the surface (Note that $B^* = \sigma T^4$)

Temperature structure in a gray atmosphere

z-axis = optical depth

z-axis = altitude

$$\tau = \tau_0 \left(\frac{p}{p_{ref}}\right)^{n_p}$$

n_p = 1–2

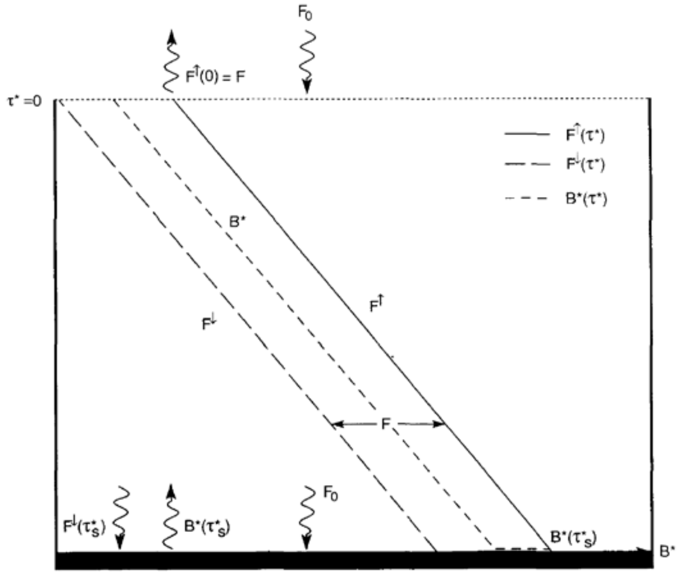

Figure 8.20 Upwelling and downwelling fluxes and emission in a gray atmosphere that is in radiative equilibrium with an incident SW flux F_0 and a black underlying surface. *Note:* the emission profile is discontinuous at the surface.

Salby (1996)

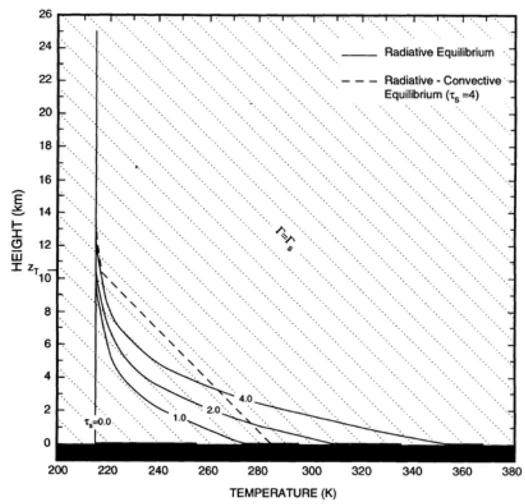

Figure 8.21 Radiative equilibrium temperature (solid lines) for the gray atmosphere in Fig. 8.20, with a profile of optical depth representative of water vapor (8.69), presented for several atmospheric optical depths τ_s. Saturated adiabatic lapse rate (dotted lines) and radiative–convective equilibrium temperature for $\tau_s = 4$ (dashed line) superposed.

Radiative-convective equilibrium

The radiative equilibrium temperature profile can be unstable at low altitudes.

Assumptions for calculating convective adjustment:

- Vertical convection transports heat vertically, leading to an adiabatic lapse rate (troposphere).
- Above this convective region, the temperature profile remains to be the radiative equilibrium one (stratosphere).
- The surface temperature becomes equal to the atmospheric temperature at the bottom.
- The surface temperature is adjusted so that the upward energy flux

$$F^{\uparrow}(\tau^*) = B^*(T_S)\exp(\tau^* - \tau_s^*) - \int_{\tau_S^*}^{\tau^*} \exp(\tau^* - \tau')B^*(T(\tau'))d\tau'$$

becomes equal to the one for radiative equilibrium

$$F^{\uparrow}(\tau^*) = \frac{F^{sum} + F^{net}}{2} = \frac{F^0}{2}(\tau^* + 2)$$

at the top of the troposphere.

Radiative convective equilibrium
for Earth's atmosphere
(Manabe & Strickler 1964)

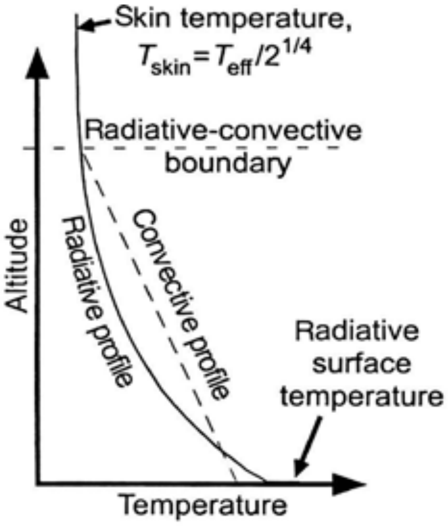

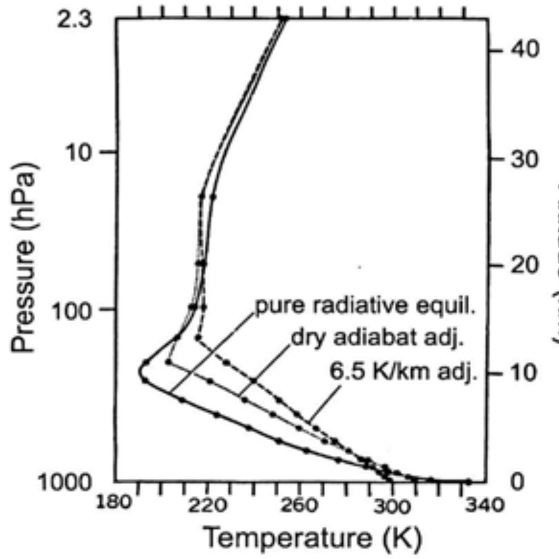

Catling & Kasting (2017)

Radiative-convective equilibrium solution for Venusian atmosphere
(Pollack et al. 1980)

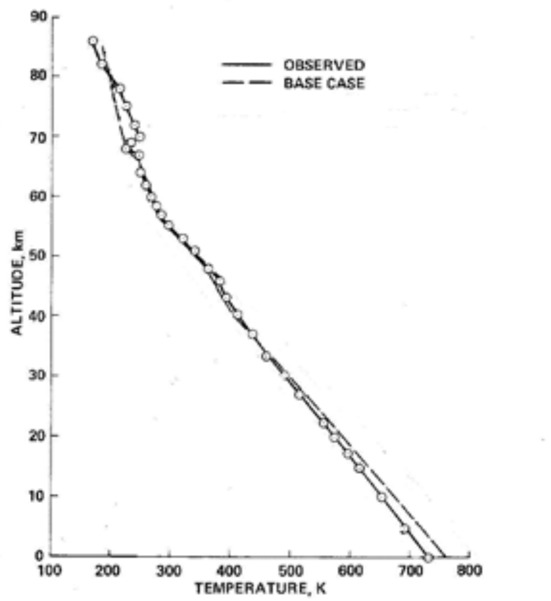

Fig. 2. Comparison between the observed temperature structure of Venus' lower atmosphere and that of several models, which are described in the main text.

Net downward solar flux
(Moroz et al. 1985)

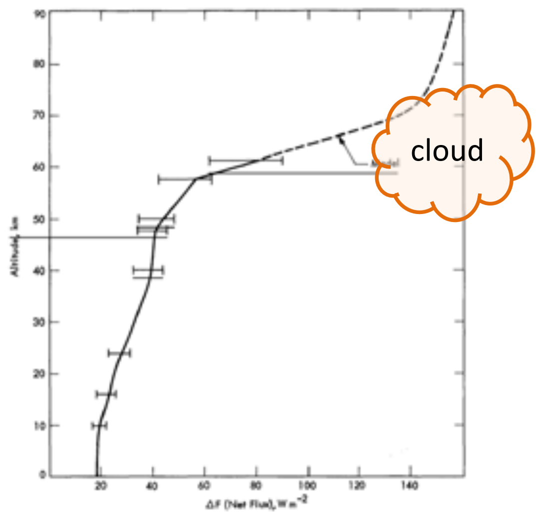

Figure 6-13. Globally Averaged Model of Total Solar Flux

Radiative-convective equilibrium solution for Martian atmosphere

without dust

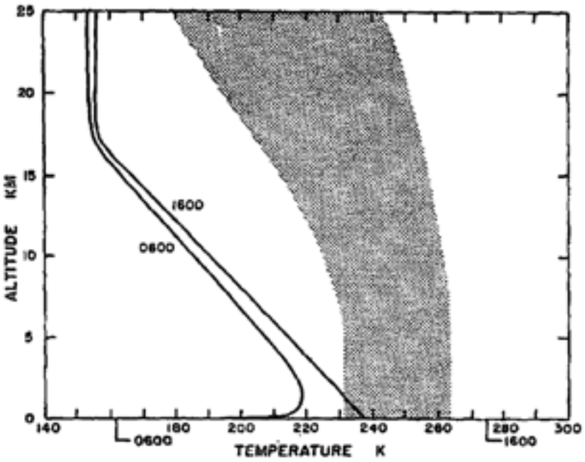

FIG. 1. Martian temperature calculations. The stippled area represents temperatures reported by Kliore *et al.* (1972) and Hanel *et al.* (1972). The lines are theoretical profiles for a pure CO_2 atmosphere, at 1600 and at 0600 hours (the coldest time). Both theory and observation refer to mid-latitude summer conditions. The tags indicate the ground temperatures. In the case of the 1600 theoretical profile a strong boundary layer is indicated.

with dust

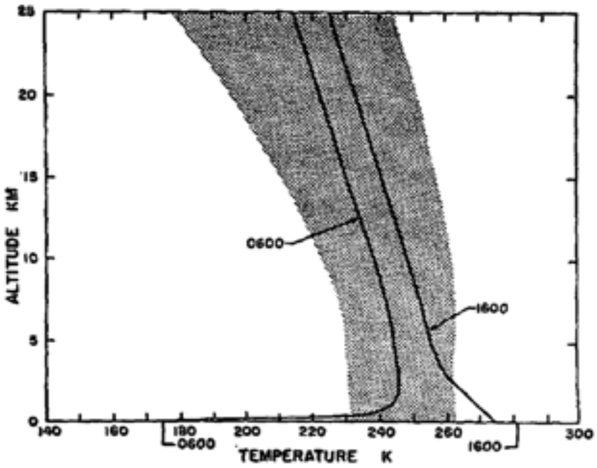

FIG. 2. Same as Fig. 1 except that the atmosphere contains an extra solar absorber, evenly mixed with the atmosphere at all levels, and having an optical depth of 0.10 at all wavelengths. Note the weak boundary layer at 1600.

Gierasch & Goody (1972)

Internal heat of gas giants

Internal heat sources include the rainout of helium-rich droplets and, possibly, continued Kelvin-Helmholtz contraction.

The Kelvin–Helmholtz mechanism is an astronomical process that occurs when the surface of a star or a planet cools. The cooling causes the pressure to drop and the star or planet shrinks as a result.

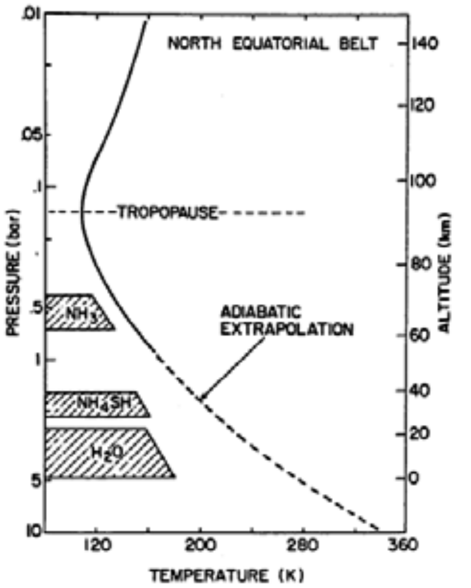

Fig. 1.26 Jovian temperatures and schematic cloud structure, based primarily on Voyager infrared data. The height scale starts at the cloud base, approximately 5 bars. [After KUNDE *et al.* (1982).]

Chamberlain & Hunten (1987)

TABLE 1.3 *Characteristics of the Jovian Planets*

	Jupiter	Saturn	Uranus	Neptune
Mean density (g/cm³)	1.34	0.70	1.58	2.30
Effective temperature (°K)	124.4	95.0	58	55.5
Equilibrium temperature (°K)	109.5	82.3	57	46
Total flux/solar heat	1.668	1.78	<1.3	1.1
Internal flux (erg cm^{-2} sec^{-1})	5444	2000	<180	285
Adiabatic lapse rate (°K/km)	1.9	0.84	0.85	0.86
Tropopause temperature (°K)	105	85	54	52
Tropopause pressure (mbar)	140	80	100	200
Exospheric temperature (°K)	700–1000	420	700	—

- Outward thermal flux > Incoming solar flux (Jupiter, Saturn)
- The Earth's internal heat flux is 1/40000 of the Incoming solar flux. This heat comes from a combination of residual heat from planetary accretion and heat produced through radioactive decay.

Heating of the upper atmosphere

Solar spectrum

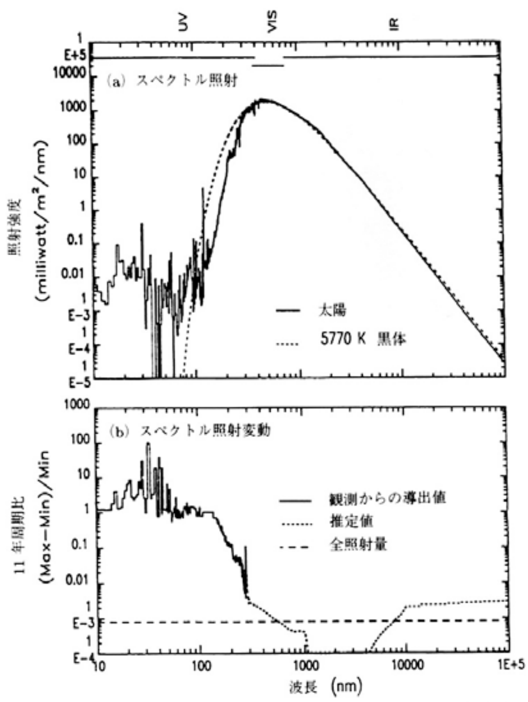

（ブレッケ，超高層大気物理学）

Structure of the solar atmosphere

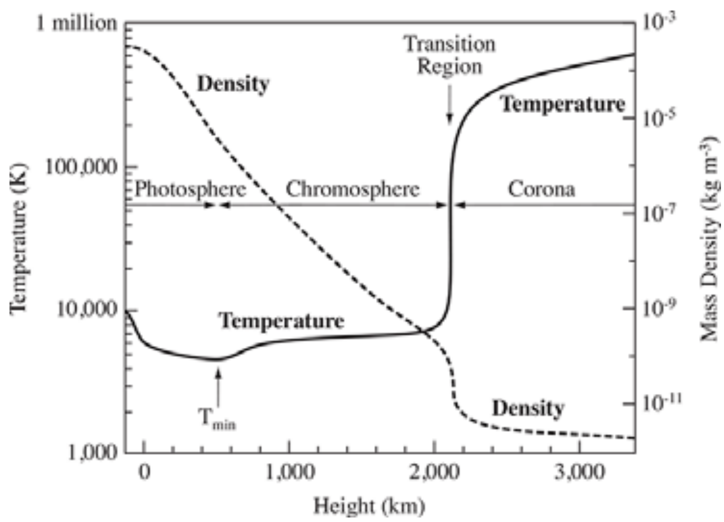

(Eugene Avrett, Smithsonian Astrophysical Observatory) chromosphere

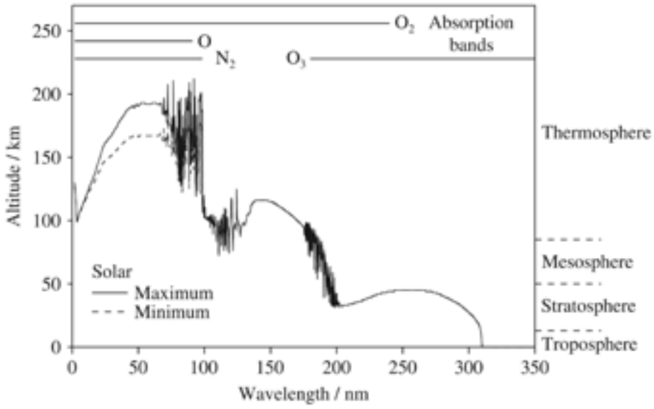

The altitude of unit optical depth for vertical solar radiation. The principal absorption bands are shown. Adapted from Meier (1991); an early version of this figure appeared in Herzberg (1965). Figure courtesy of Dr J. Lean and Dr R. Meier.

(Andrews 2010)

Energy balance of the thermosphere

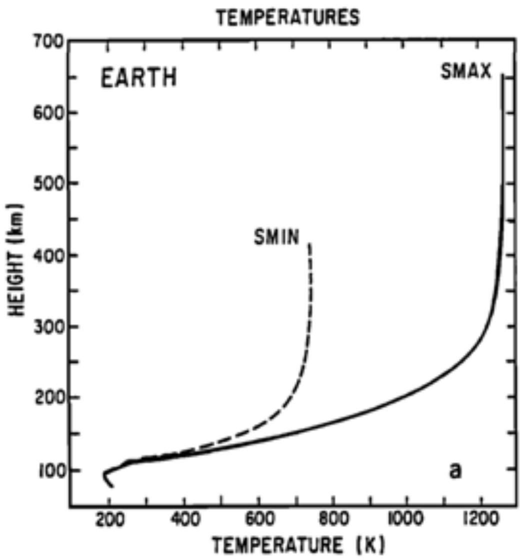

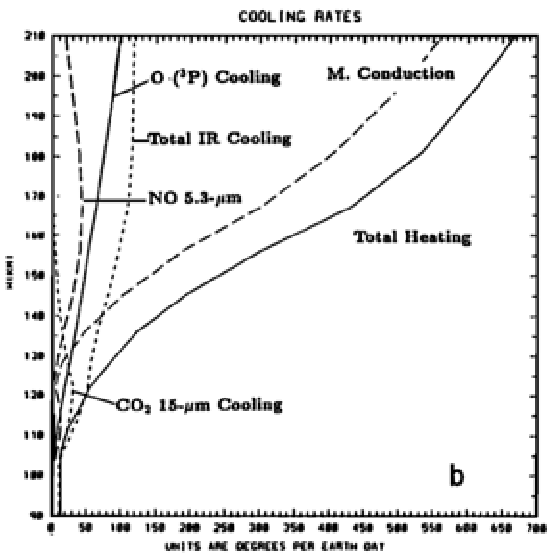

Bougher et al. (1994)

Molecular diffusion coefficient (for CO_2) (Chapman and Cowling 1970)

$$K = 1.38\times10^5 \cdot \frac{1}{\rho} \cdot \left(\frac{T}{273}\right)^{0.933}$$

ρ : Atmospheric density
T : Atmospheric temperature

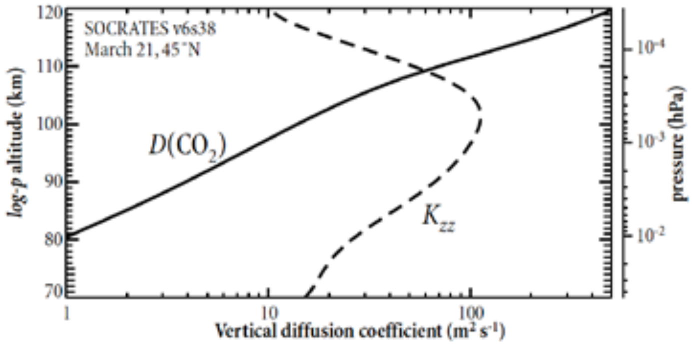

Figure 1. Vertical profiles of the eddy diffusion coefficient and the CO_2 molecular diffusion coefficient, using the SOCRATES baseline model. Latitude 45°North, equinox (March 21), solar minimum conditions.

Chabrillat et al. (2002)

Composition of Earth's upper atmosphere

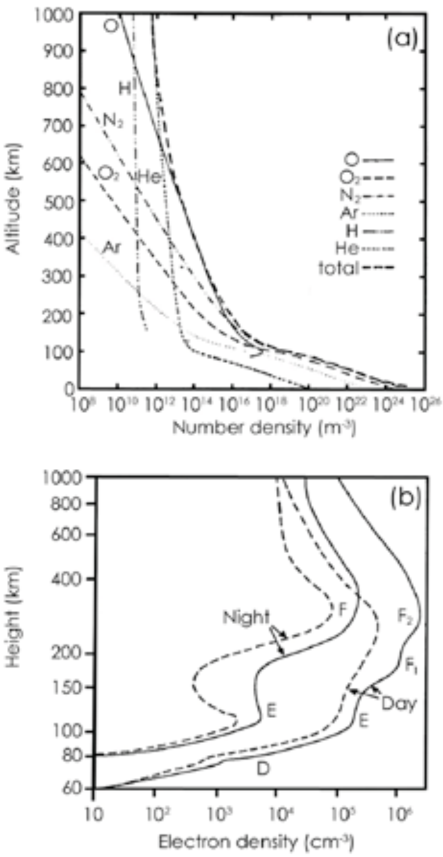

Borderick, 2010

Homopause levels

Table 1.1 Homopause levels. (Sources: Atreya *et al.* (1991), p. 145; Atreya *et al.* (1999).)

Planet	Altitude (km)	Pressure (μbar)	Number density (molecules cm^{-3})
Venus	130–135	0.02	7.5×10^{11}
Earth	~100	0.3	10^{13}
Mars	~130	0.002	10^{10}
Jupiter	~385 above 1 bar level	1	1.4×10^{13}
Saturn	~1140 above 1 bar level	0.005	1.2×10^{11}
Titan	800–850	~0.0006	2.7×10^{10}
Uranus	~354–390 above the 1 bar level	~20–40	$1\text{–}2 \times 10^{15}$
Neptune	~586–610 above the 1 bar level	~0.02	10^{13}

Catling & Kasting (2017)

Mars and Venus thermospheres

Mars

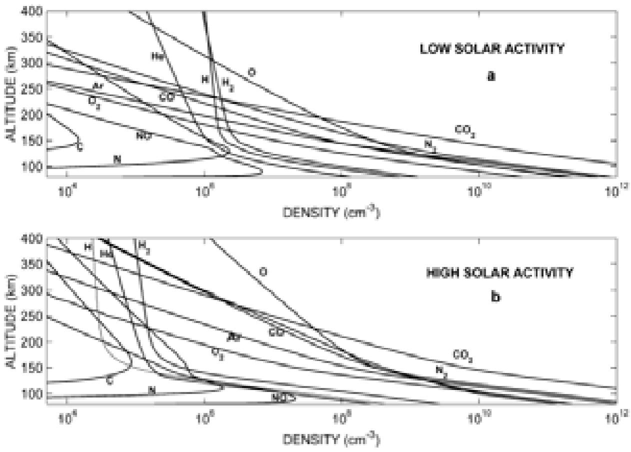

(Bakalian et al. 2006)

Venus

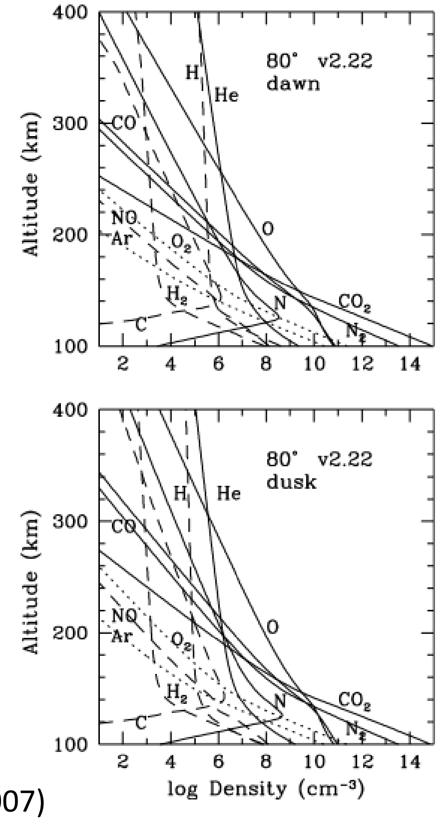

(Fox & Kasprzak, 2007)

Thermospheres of the terrestrial planets

(Bougher et al. 1994)

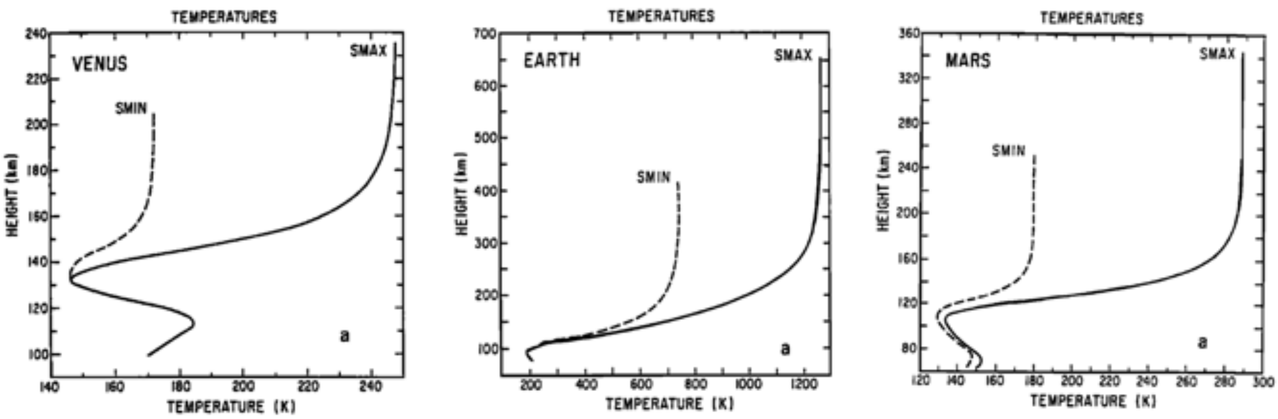

Thermospheric temperature

Earth: 1000 K Venus: 250 K Mars: 270 K

The coolants in Earth's thermosphere, CO_2 and NO, are relatively ineffective because of their low concentrations.
On Venus and Mars, the atmospheres are almost CO_2, which makes the upper atmospheres cold through efficient radiative cooling.

Radiative energy balance at each altitude

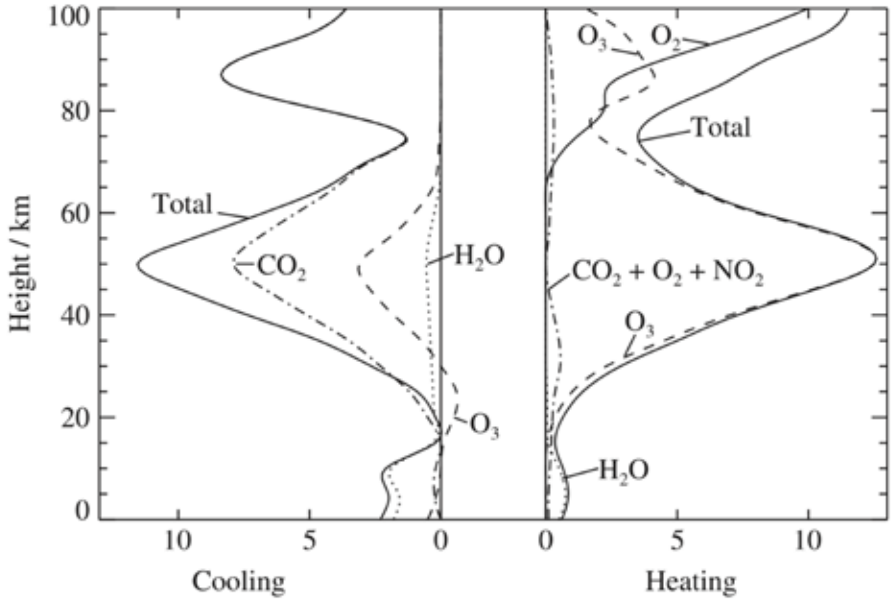

Global-mean vertical profiles of the short-wave heating rate and the long-wave cooling rate, in K day^{-1}, including contributions from individual gases. Adapted from London (1980).

(Andrews 2010)

Jovian thermospheric temperature

22,876 SEIFF ET AL.: THERMAL STRUCTURE OF JUPITER'S ATMOSPHERE

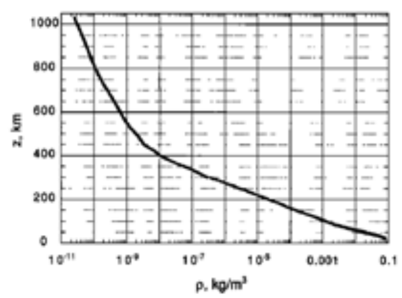

Figure 26. Density of the upper atmosphere as a function of altitude, derived from measured probe decelerations. A major change in density scale height occurred between 350 and 550 km. This coincides with the onset of diffusive separation. The steeper slope above 550 km indicates a major warming of the upper atmosphere.

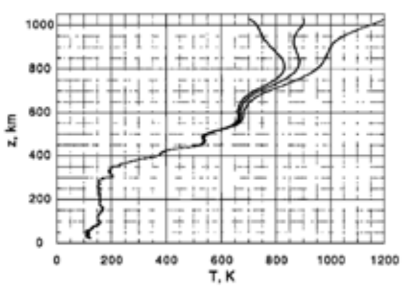

Figure 28. Temperature structure of the upper atmosphere calculated from measured densities, derived pressures, and the mean molecular weight profile of Figure 19. The effect of three widely differing temperature assumptions at the initial altitude is shown. The three profiles effectively converge at 750 km altitude. Waves in the thermal structure and the deep isothermal layer below 300 km are conspicuous.

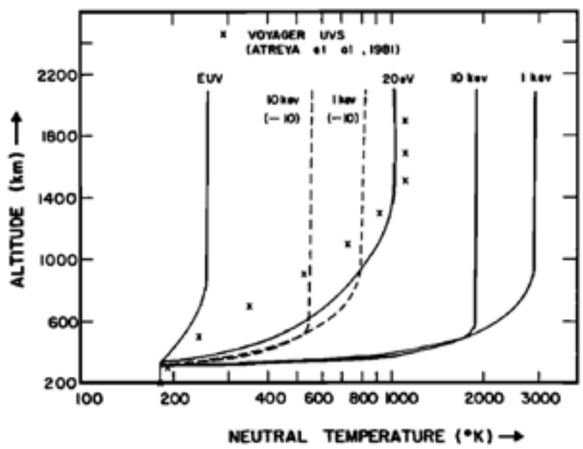

Fig. 16. Neutral temperature as a function of altitude for several cases of interest. The EUV results use only photoelectrons as a heat source. The 20-eV case considers the heating due to 20-eV electrons with an energy flux equal to 0.5 ergs $cm^{-2}s^{-1}$. The 1- and 10-keV auroral electron cases show the effects of electron heating from 1- and 10-keV electrons with an energy flux of 10 ergs cm^{-2} s^{-1} and for auroral heating rates diluted by a factor of 10 to illustrate the possible global effects of auroral heating. The Voyager UVS stellar occultation-derived profile is shown by the crosses.

Waite et al. (1983)

The temperature rise across the thermosphere due to solar UV heating is predicted to be <100 K.

A much stronger source of heat must be present.

- Precipitating electrons ?
- Wave heating (gravity wave, acoustic wave) ?

Vertical structures of planetary atmospheres

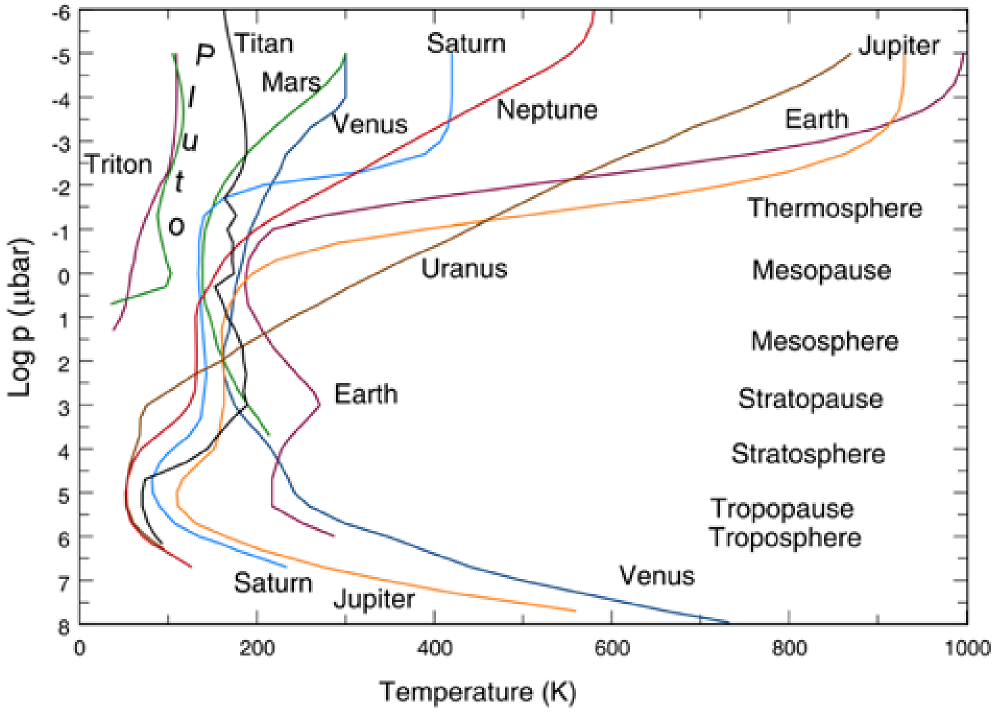

(Mueller-Wodarg et al.)